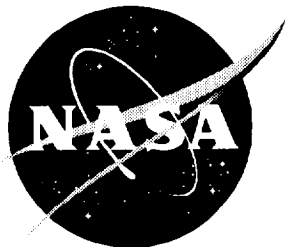NASA/TP-1999-209124

Modeling and Validation of a Navy A6-Intruder Actively Controlled Landing Gear System

Lucas G. Horta, Robert H. Daugherty, and Veloria J. Martinson
Langley Research Center, Hampton, Virginia

May 1999

Abstract

Concepts for long-range air travel are characterized by airframe designs with long, slender, relatively flexible fuselages. One aspect often overlooked is ground-induced vibration of these aircraft. This paper presents an analytical and experimental study of reducing ground-induced aircraft vibration loads by using an actively controlled landing gear. A facility has been developed to test various active landing gear control concepts and their performance. The facility uses a Navy A6-Intruder landing gear fitted with an auxiliary hydraulic supply electronically controlled by servo valves. An analytical model of the gear is presented, including modifications to actuate the gear externally, and test data are used to validate the model. The control design is described and closed-loop test and analysis comparisons are presented.

1. Introduction

Market analysis of future commercial air travel has identified a significant trans-Pacific market for supersonic transports. Fuselage and wing design of these transports is governed primarily by aerodynamics and associated structural loads. Placement and sizing of the landing gear occur at a later stage in the design process, with design constraints such as braking requirements, turning radius for ground handling, ground clearance during rotation, and weight distribution as the main criteria (ref. 1).

Long, slender, flexible fuselage configurations, especially those with a long overhang from the nose gear to the cockpit, are susceptible to ground-induced vibration problems, particularly those produced by operating over long-period, low-amplitude elevation disturbances on runways. Although in-flight vibrations are also a concern, the work discussed herein will address the mitigation of vibrations transmitted from the ground to the aircraft fuselage. The mitigation is accomplished by embedding a control system directly into the landing gear.

This paper presents results from an activity at Langley Research Center that investigated three aspects of actively controlled landing gear: analytical modeling, control system design, and experimental validation. This work attempts to improve the fidelity of analytical models so that they can be used for control design and experimental demonstration of various control philosophies. Development of an experimental facility that permits realistic concepts that can be transferred to commercial applications is also a goal.

Development of landing gear analysis dates back to the late 1950's (ref. 2). Work has included numerical simulation techniques and experimental measurements to validate the various computer programs. A significant volume of the work available in the literature deals with military aircraft requiring accurate prediction of taxi loads over repaired, bomb-damaged runways (refs. 3–6). A computer simulation program named HAVE BOUNCE (ref. 6) was developed to simulate the dynamic response of military aircraft over bomb-damaged runways. To validate the computer code, model validation was performed at the Aircraft Ground-Induced Loads Excitation (AGILE) (ref. 7) test facility at Wright-Patterson Air Force Base. Recently, attention has focused on ride quality during taxi, takeoff, and landing (refs. 8 and 9). A simulation program developed by Stirling Dynamics (refs. 8 and 9) is a good example of new simulation capabilities. This particular computer simulation program has been validated with data from commercial transports in Europe.

Because the primary design driver in landing gear design is impact loading, landing gears are typically tuned passively for impact loading upon landing. Ross and Edson (refs. 10 and 11) are among the first to consider an actively controlled landing gear to reduce landing loads. Their work is the basis for the actively controlled landing gear concept described in this paper. Ross and Edson demonstrated the benefits of using an actively controlled landing gear system to reduce impact loads upon landing and while traversing bomb-damaged runways. Work by Freymann (ref. 12) demonstrated analytically and experimentally the benefits of actively controlled landing gear in reducing landing loads and vibrations under various runway profiles. In reference 13, Daniels presented analysis and test results for a Navy A6-Intruder landing gear system. This paper discusses an extension of the work in reference 13 to incorporate active controls. An A6-Intruder gear was used in the laboratory because it was readily available. Necessary modifications to the gear are described along with the facility used in the experimental validation phase.

2. Symbols

A_L lower chamber cross-sectional area, ft^2

A_o effective orifice area, ft^2

A_R snubber annulus area, ft^2

A_s snubber orifice area, ft^2

A_u upper chamber cross-sectional area, ft^2

C_c servo valve effective discharge coefficient

C_d main orifice discharge coefficient

C_{dS} snubber discharge coefficient

C_t tire damping, lbf-s/ft

c arbitrary scalar constant

D_L diameter of lower chamber, ft

D_o effective diameter of main orifice, ft

D_{op} orifice plate hole diameter, ft

D_p piston diameter, ft

$D_{pin}(X_s)$ metering pin diameter, ft

D_R snubber chamber effective diameter, ft

D_s snubber orifice diameter, ft

D_u diameter of upper chamber, ft

$d(s)$ disturbance signal, ft/s^2

E_1	derived quantity defined for equation (A15)
F_{ow}	friction force defined in equation (A28), lbf
F_t	tire force, lbf
f	friction force, lbf
$G(s)$	system transfer function, $1/\text{ft}^2$-s
g	gravitational acceleration, 32.2 ft/s^2
K_t	tire stiffness, lbf/ft
$k(s)$	controller transfer function, ft^2-s
L	lift forces, lbf
L_u	upper chamber total length, ft
l	axle off-center distance, ft
M_L	piston and tire mass, lbm
M_u	upper mass, lbm
$m(s)$	sensor noise, ft/s^2
N	normal cylinder force, lbf
P_{High}	reservoir high pressure, lbf/ft^2
P_L	lower chamber pressure, lbf/ft^2
P_{Low}	reservoir low pressure, lbf/ft^2
P_{ni}	nitrogen charge pressure, lbf/ft^2
P_s	snubber chamber pressure, lbf/ft^2
P_u	upper chamber pressure, lbf/ft^2
Q_c	volumetric flow due to servo valve actuation, ft^3/s
Q_{ideal}, Q_{real}	ideal and actual flow rates, ft^3/s
Q_o	flow rate through orifice plate, ft^3/s
Q_s	flow rate through snubber orifice plate, ft^3/s

$r(s)$	reference signal, ft/s^2
(s)	indicates Laplace transform
$U(t)$	inertial reference ground input, ft
V_{liq}	total volume of hydraulic fluid, ft^3
V_{ni}	initial nitrogen volume, ft^3
V_T	upper chamber total volume, ft^3
v	fluid velocity, ft/s
X_a	lower mass inertial reference position, ft
X_{ni}	initial nitrogen level, ft
X_s	piston stroke, ft
X_{wg}	upper mass inertial reference position, ft
x_c	command voltage, V
$x(s)$	error command, ft/s^2
$y(s)$	measured output, ft/s^2
z	streamline elevation, ft
β	half thickness of lower bearing, ft
γ	polytropic gas constant
μ	friction coefficient
ρ	density, lbm/ft^3
ϑ	specific weight, lbf/ft^3

Superscripts:

i	indicates inflow
o	indicates outflow

Subscripts:

1,2	points along streamline
L	refers to lower mass

u	refers to upper mass
$(\ddot{\ })$	refers to second derivative with respect to time
$(\dot{\ })$	refers to first derivative with respect to time

3. Analytical Model

To extend the work by Ross and Edson (ref. 10), this research discusses an independent development of a main landing gear mathematical model. The nonlinear equations of motion were developed for a telescoping main gear modified with an external hydraulic system for actuation and control of the gear. Specific details of the landing gear were taken from technical drawings supplied by the Grumman Company.

Figure 1 shows a schematic of a landing gear used in the development of the equations of motion. This schematic is representative of a general telescoping main landing gear. The model includes the aerodynamic lift L on the airplane, the mass of the airplane's fuselage, lumped with the mass of the
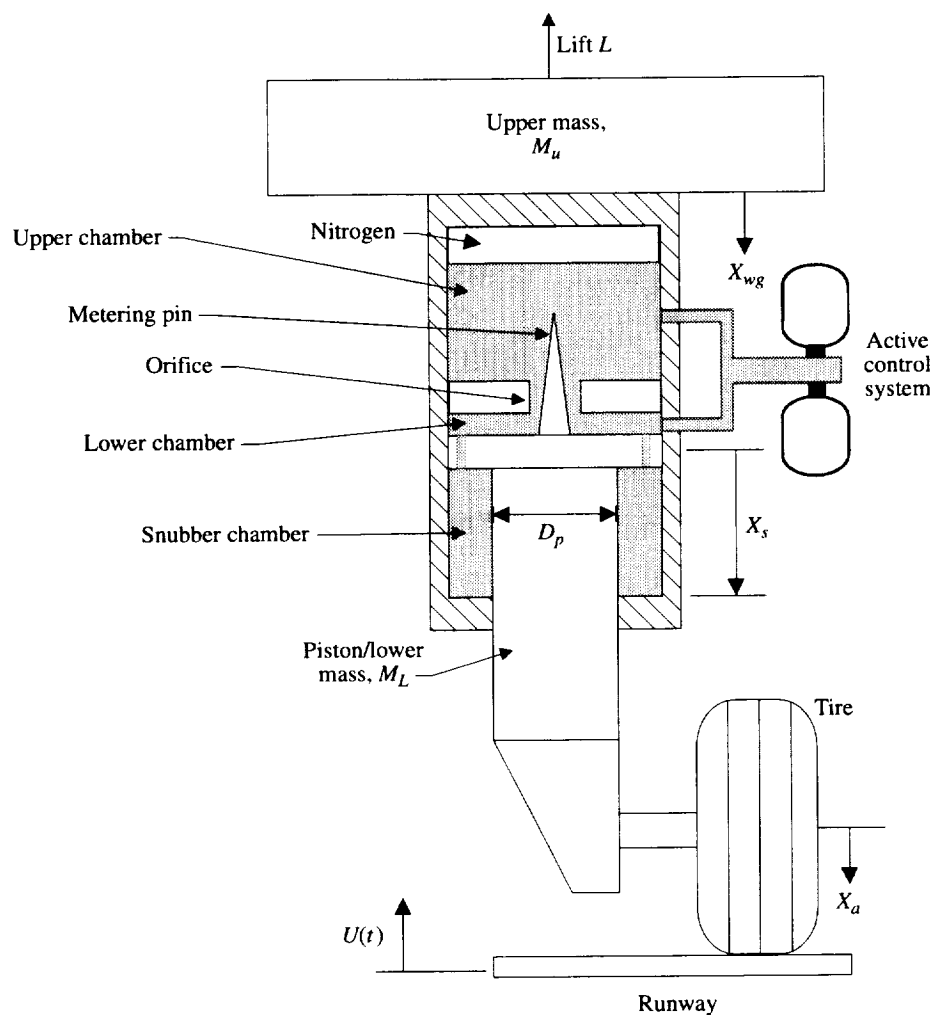

Figure 1. Schematic of telescoping main landing gear.

5

main cylinder as M_u, and the mass of the piston lumped with the mass of the tire as M_L. The inertial position of the upper mass is X_{wg} with zero value when the gear is fully extended and the tire is just touching the ground. From this same configuration, X_a is the position of the lower mass taken as zero at the axle of the tire. When the gear is compressed, X_a measures the deflection of the tire to an inertial reference ground input $U(t)$. Part of the upper cylinder chamber is filled with compressed nitrogen to provide the system with a spring. The cross-sectional area of the upper chamber is denoted by A_u and the corresponding pressure is P_u. Likewise, the lower chamber has the cross-sectional area denoted A_L and a corresponding pressure P_L. Hydraulic fluid moves between the upper and lower chambers through an orifice plate with a hole of diameter D_{op}. A tapered pin attached to the piston, known as a metering pin, is used to obstruct the flow and effectively vary the orifice diameter as the pin moves through the orifice. The pin diameter is a function of X_s and is denoted as $D_{pin}(X_s)$. Hydraulic fluid reaches the snubber chamber through several orifices of diameter d_s. In the snubber chamber, the annulus area is denoted by A_R and the pressure is P_s. The diameter of the piston is D_p. Some of the actual dimensions are defined in table 1. The figure denotes entry-exit ports in the upper and lower chambers for the exchange of hydraulic fluid used by the active control system. Tire spring and damping coefficients are denoted by K_t and C_t.

Table 1. Properties and Dimensions for the Navy A6-Intruder

Landing gear properties	Dimensions
D_u	0.1524 m, (6 in.)
D_L	0.1524 m, (6 in.)
D_s	0.0041 m, (0.1614 in.)
D_p	0.1397 m, (5.5 in.)
D_o	0.02859 m, (1.125 in.)
L	0.3832 m, (15.087 in.)
M_L	145.1 kg, (319.22 lbm)
M_u	4832.7 kg, (10609.94 lbm)
γ	1.1
β	5 cm, (2 in.)
ρ	912 kg/m^3, (1.22 × 10^8 lbm/in^3)

Figure 2 shows the forces acting on the upper mass. Balancing the forces acting on the upper mass yields the following equation:

$$M_u \ddot{X}_{wg} = M_u g - L - P_u A_o - P_L(A_L - A_o) + P_s A_R - f = F_1 - f \tag{1}$$

where F_1 is a newly defined term in equation (1), g is the gravitational acceleration, and f is the friction force between the piston and the cylinder wall. All other terms were described previously. This equation assumes that the hydraulic fluid pressure in the upper cylinder is identical to the nitrogen pressure. Also, in this development, the variable A_o, the main orifice area, shows that the metering pin is included; that is, it is a variable cross-sectional area depending on the stroke of the piston.

Figure 3 shows the forces acting on the piston. By adding the forces on the lower mass (piston), the force balance equation is

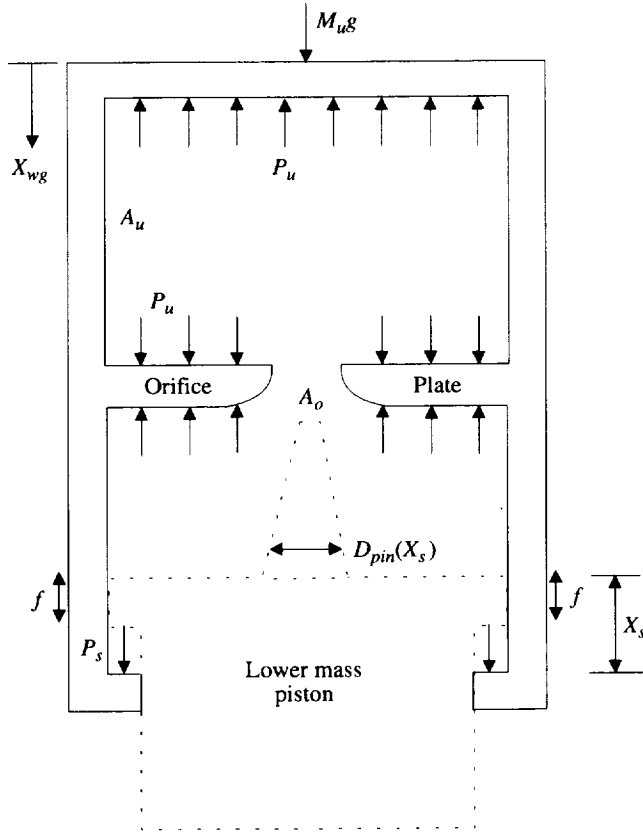$$M_L \ddot{X}_a = M_L g + P_L(A_L - A_s) - P_s(A_R - A_s) - F_t + f = F_2 + f \tag{2}$$

6

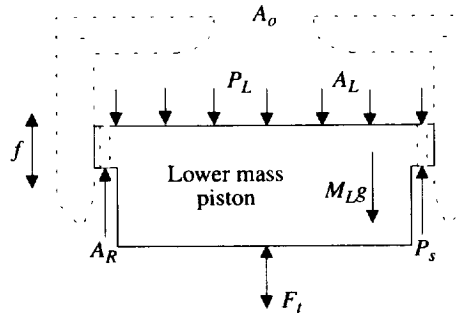Figure 2. Schematic of upper mass and main cylinder.

Figure 3. Schematic of lower mass.

where F_2 is newly defined in equation (2); F_t is the force that is transmitted through the tire from the ground and has the form

$$F_t = K_t(X_a + U) + C_t(\dot{X}_a + \dot{U})$$

where the tire force is defined as a linear function of tire stiffness and damping. The tire stiffness and damping coefficients are obtained by linearizing the behavior of the tire about its nominal operating point. Because all pressures are functions of stroke, a more convenient coordinate to use is stroke. Defining the stroke coordinate as $X_s = X_{wg} - X_a$, equations (1) and (2) can be written as

7

$$M_u \ddot{X}_{wg} = F_1 - f$$

$$M_L \ddot{X}_s = \frac{M_L}{M_u} F_1 - F_2 - \left(1 + \frac{M_L}{M_u}\right) f \qquad (3)$$

The discussion so far relates forces F_1 and F_2 to the corresponding pressures. Chamber pressures must now be related to displacement and velocity of the gear. Appendix A discusses the relationship of pressure to piston motion as well as pressure control using external tanks. Gear actuation using external tanks enables the design of control strategies to reduce unwanted motion due to ground inputs. In the following, a description of a general approach for control design is presented.

4. Control System Design

To control the motion of the landing gear, hydraulic fluid from auxiliary tanks is used in conjunction with electronically controlled valves to actuate the gear. The goal for control design is to minimize disturbance propagation from the ground into the fuselage. To aid the discussion on control design methodology, consider a linearized representation of the landing gear and servo valves that are transformed by using Laplace's transform into $G(s)$. Using feedback control, as indicated in figure 4, one can design a controller $k(s)$ to command the servo valves.

Define $r(s)$ as an arbitrary input reference signal, $d(s)$ as an unknown external disturbance, $y(s)$ as the controlled response, and $m(s)$ as sensor noise. After some block diagram manipulation, the controlled response is given by

$$y(s) = [I + G(s)k(s)]^{-1}[d(s) + G(s)k(s)r(s) - G(s)k(s)m(s)] \qquad (4)$$

The factor $I + G(s)k(s)$ is the return difference and multiplies every term in the right-hand side of the equation. To minimize the effects of the disturbance $d(s)$ on the response, the factor multiplying the disturbance term $d(s)$ must be made small; that is, the return difference must be large, $G(s)k(s) \gg 1$, in the frequency range of interest. Because $G(s)$ is fixed, the control designer's task is to maximize the return difference value while maintaining the stability of the system. To ensure a stable design, the Nyquist criterion is used for this single-input, single-output problem. Because the landing gear behavior is highly nonlinear, one must examine bounds of variations in the system dynamics to ensure a stable design. The Nyquist criterion was computed experimentally to assess stability and gain margins of the design. These techniques provide tremendous insight into design philosophy and stability analysis, although their application to nonlinear systems is limited.

5. Experimental Facility

Figure 5 shows a Navy A6-Intruder main landing gear installed underneath a drop carriage in the standard vertical position. A connecting plate was fabricated to allow for normal mounting of the gear to the plate, and the plate was then rigidly connected to the drop carriage. The drop carriage is a truss structure that weighs about 4.5 tons and allows unrestrained vertical motion. The drop carriage rests on the landing gear. This mass simulates the rigid portion of the aircraft mass carried by the gear. Once the gear is loaded, a shaker table is used to input forces into the gear. Hydraulic lift cylinders, powered by a hydraulic pump, are used to lift the drop carriage and unload the gear. Once the gear has been lifted, the ability exists to lock the gear in that position with hydraulic valves.
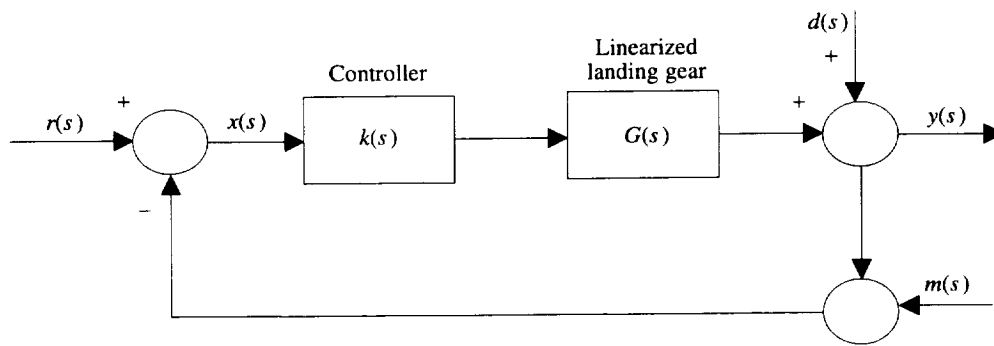
8

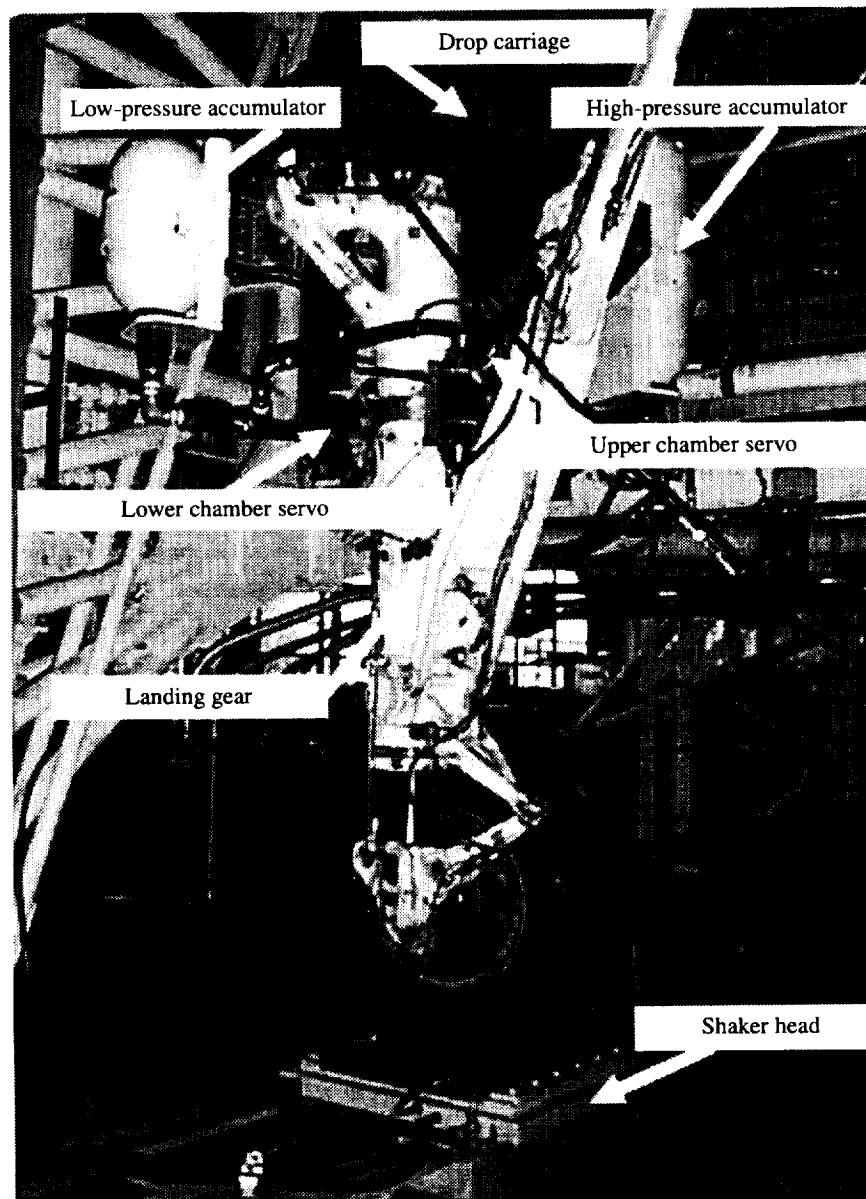Figure 4. Block diagram of control system.

Figure 5. Test setup for validation of analysis model and control system.

The hydraulic shaker table was built specifically for the task of actuating landing gears. The specifications included the capability to perform a 1-in. step bump in 2 ms while bearing 12000 lb mass. Input waveforms such as $1 - \cos(x)$, $\sin(x)$, trapezoidal with user-selected rise time, and a sawtooth waveform are all accurately reproduced by the shaker table. General profiles using runway elevation versus time data are also reproduced well for low frequencies. The shaker table is capable of applying dynamic forces up to 12 000 lbf on the test mass and allows actuator movement of 6 in.

The landing gear was modified in a number of ways. Two electrohydraulic servo valves were attached to the outside of the landing gear on flat areas that had been machined on the outer cylinder of the gear. One valve was located above the orifice plate of the gear (in the upper chamber), and the other valve was located below the orifice plate (in the lower chamber). Holes were machined into the gear so that the valves could transfer pressurized hydraulic fluid either into or out of the desired chamber. Both valves were designed to have flow rates of at least 26 gal/min at 600 psi with a response approaching 100 Hz. A high-pressure accumulator was mounted on the upper mass (drop carriage) and was kept charged to a pressure approximately twice that of the static-loaded charge pressure in the landing gear. A low-pressure accumulator was also installed so that when desired, pressurized hydraulic fluid in the landing gear could be directed there, reducing the transient back pressure that would tend to restrict the outward flow of hydraulic fluid. The low-pressure accumulator was maintained at essentially atmospheric pressure. Ultimately, the low-pressure accumulator was attached to an atmospheric pressure reservoir where the pump used to supply the high-pressure accumulator was located. The system was thus pressure balanced evenly around the nominal static, loaded charge pressure of the landing gear, permitting roughly equal flow rates into or out of the gear at similar servo command levels.

The piston head of the landing gear was also modified. Normally, such a landing gear has a snubber chamber that is designed to limit the speed of piston extension to prevent a significant "bottoming out" shock on the gear components such as might occur after a catapult during an aircraft carrier launch. Thus, normally the hydraulic damping characteristics of the gear vary depending on the direction of piston travel. In this experiment, it was desirable to remove the "snubber" effect so that the damping behavior was more even in both directions. To that end, a ring mounted directly under the piston head, which normally acts as a directional valve and restricts hydraulic fluid motion in one direction, was modified by drilling additional holes to provide equal flow past the ring, regardless of the direction of hydraulic fluid motion. These changes were accurately reflected in the modeling of the gear for analytical purposes.

The top of the landing gear was modified slightly to accept a high-strength site glass. This site glass allowed a visual indication of the proper servicing level of hydraulic fluid, prior to being pressurized with nitrogen, and saved significant time in pretest operations.

The gear was instrumented to provide the necessary information for model validation. There are two accelerometers, one placed at the upper mass and the second at the lower mass. Two potentiometers were also used, one to locate the upper mass with respect to a fixed position on the carriage and one to measure the relative position between the upper and lower masses of the gear. Two pressure transducers were used to verify some basic model assumptions, mainly that the hydraulic fluid and the gas do not mix to any significant degree after initial shaking. One pressure transducer was located just outside the charge port of the upper cylinder, and the other is embedded in the piston head. By using a strain gauge on the wheel axle, strut vertical load was inferred by measuring bending moments induced by the tire.

10

6. Test Results and Model Validation

The following section discusses experimental results from tests conducted on the landing gear system. First, the servo loop dynamics and electronics are characterized and compared with the analytical model. Second, the simulation model, which was constructed using a commercially available software, is described. Finally, test results for various open-loop and closed-loop cases are presented.

6.1. Servo Loop Dynamic Characterization

Figure 6 presents a plot of flow rate as a function of servo command. These data were measured by removing nitrogen from the unrestrained landing gear and computing flow rates by measuring piston stroke rates as a result of discrete servo commands. Tests were then conducted with the piston restrained from moving to characterize the servo loop dynamics with minimum interference from piston motion. The slope of the measured flow rate versus command gives the product $C_c\sqrt{\Delta P}$ in equations (A16) and (A17) where ΔP is the pressure difference between the supply or return and the strut internal pressure. By using these results, the servo effective discharge coefficient was calculated to be $C_c = 1.0765 \times 10^{-6}$. To compare simulated chamber pressures to test, a test was conducted using a sinusoidal sweep from 0.5 Hz to 10 Hz. Input voltages from the test were input into the simulation, and the computed frequency response for upper chamber pressure to servo command is shown in figure 7. Test results are depicted with a solid line and simulation with a dashed line. Lower chamber tests results (not shown) are similar but with slightly more phase delay between commands and internal pressure variations. The initial pressure in the chamber was recorded as 350 psi, the initial stroke was 10.3 in., and the high-pressure accumulator pressure was 750 psi. The nitrogen level was estimated to be 4.78 in. Simulation results were generated by using Simulink/Matlab (ref. 14) computer simulation code (The Mathworks, Inc., Natick, MA). The upper curve in figure 7 shows the magnitude ratio of upper pressure to input voltage as a function of frequency, whereas the lower curve shows a phase comparison. This transfer function represents the servo valve hydraulic system response at the conditions mentioned previously.
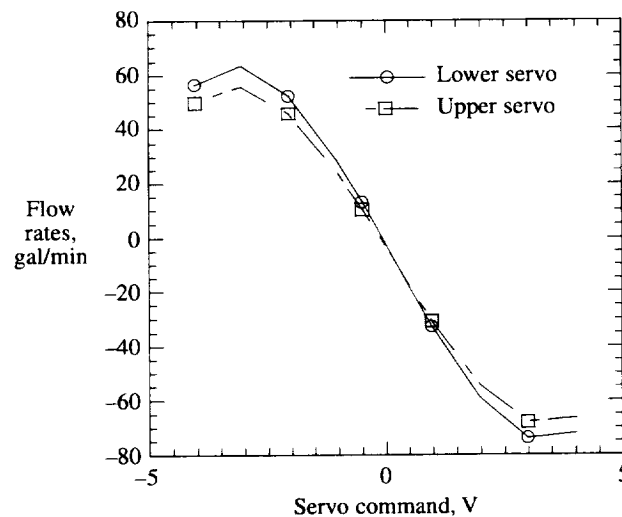

Figure 6. Flow rate as function of servo commands with unrestrained landing gear and no nitrogen.
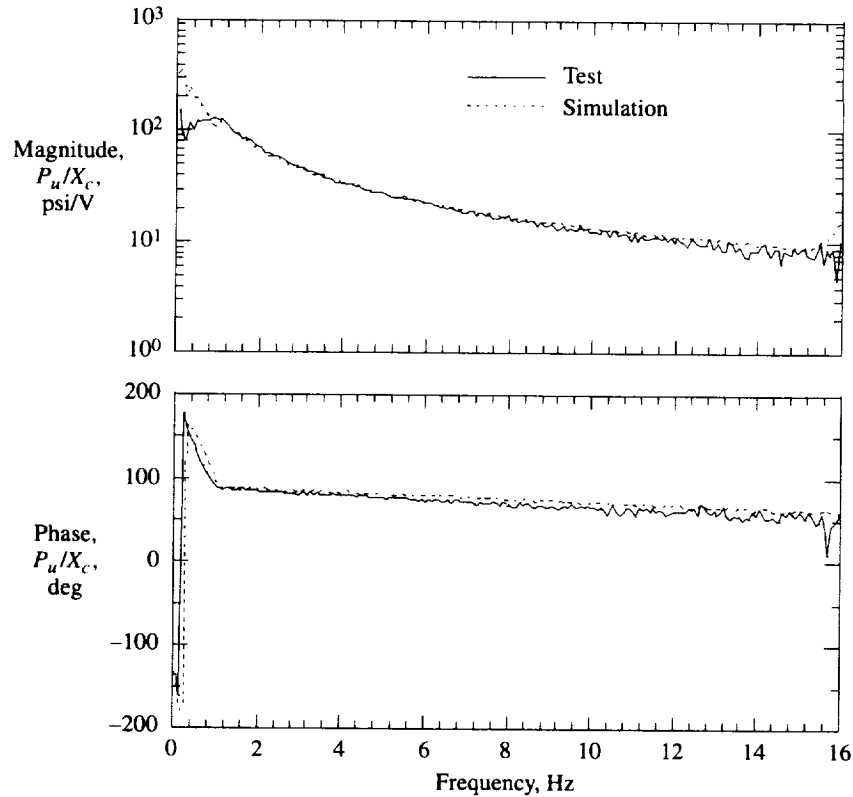
11

Figure 7. Upper chamber pressure to servo command transfer function.

6.2. Landing Gear Dynamic Characterization and Model Validation

Runway elevations and servo command voltages were the two inputs used to characterize the landing gear. Because the system is highly nonlinear, sine sweeps were the main form of excitation. Time simulations were performed with Simulink. Because the model is nonlinear, initial conditions for the different parameters have to be set properly or time integration will fail. Conditions such as upper mass position and velocity, piston stroke, stroke rate, upper chamber pressure, and nitrogen level must all be specified. In the initial design, two sensors were used to control the motion of the gear, piston stroke, and upper mass acceleration. Because the axle load signal from the strain gauge is proportional to the upper mass acceleration, the strain gauge output was used for later tests. The axle-mounted strain gauges had the additional benefit of being relatively "quiet" and avoided the more dynamic nature of acceleration measurements on stiff structures such as those observed with the upper mass accelerometer.

The controller used for all the closed-loop tests was synthesized with the aid of an experimentally determined Nyquist diagram. To compensate for phase lag of the servo valves and hydraulic system, a lead-lag compensator was used to add about 10° of lead at 1.5 Hz. Direct axle load feedback with a loop gain of 1 V/6731 lbf was used for all the closed-loop test results shown.

Shaker head position, servo-input command, piston position, upper mass position, internal pressures, and acceleration responses are compared to simulation results in figures 8 and 9. Solid lines correspond to test results and dashed lines are simulation results. The input runway elevation is a sinusoid with amplitude of 0.75 in. at a frequency of 1.5 Hz. Piston position feedback is always used to maintain interchamber leakage through the servo valve to prevent depleting the hydraulic fluid in the strut.
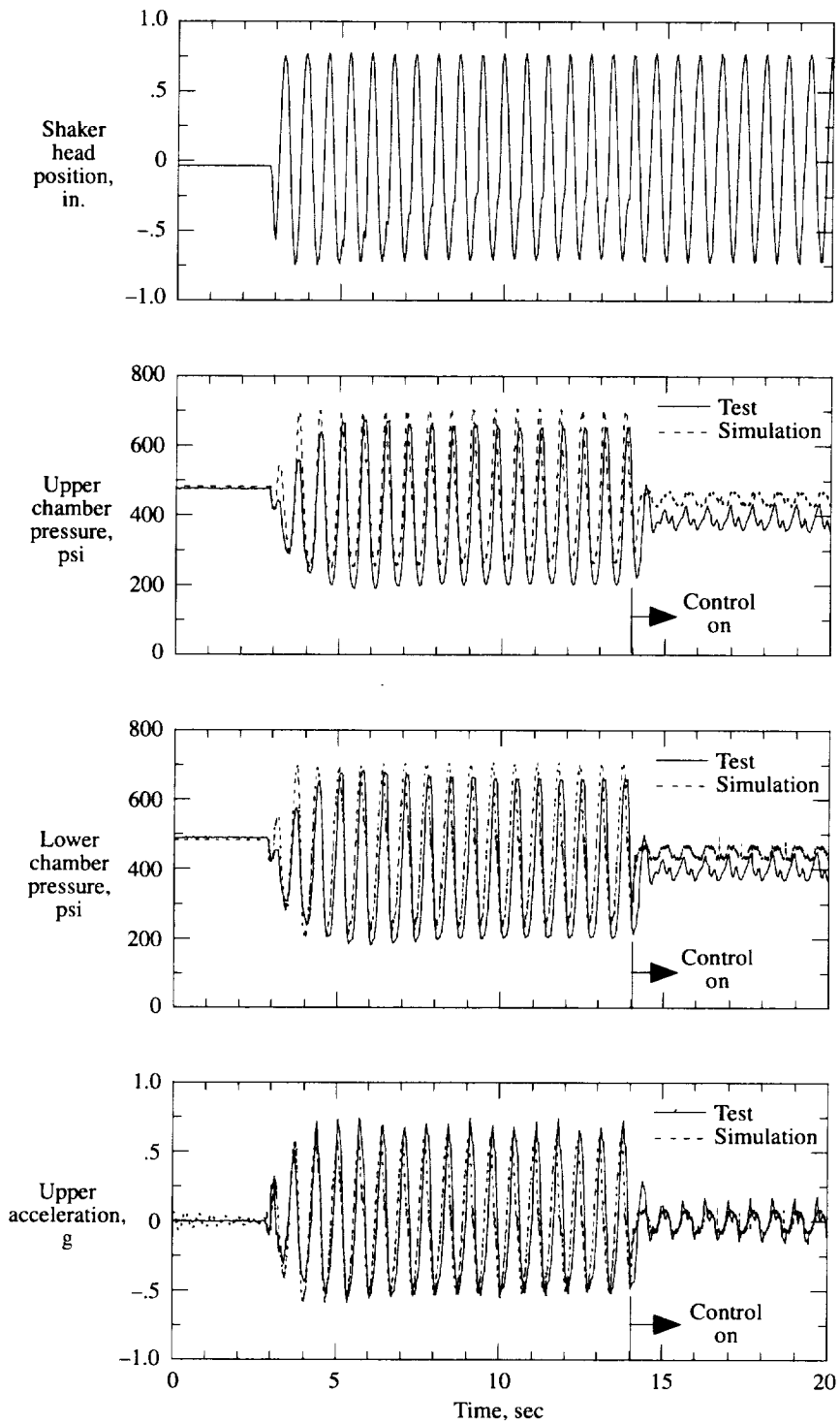
12

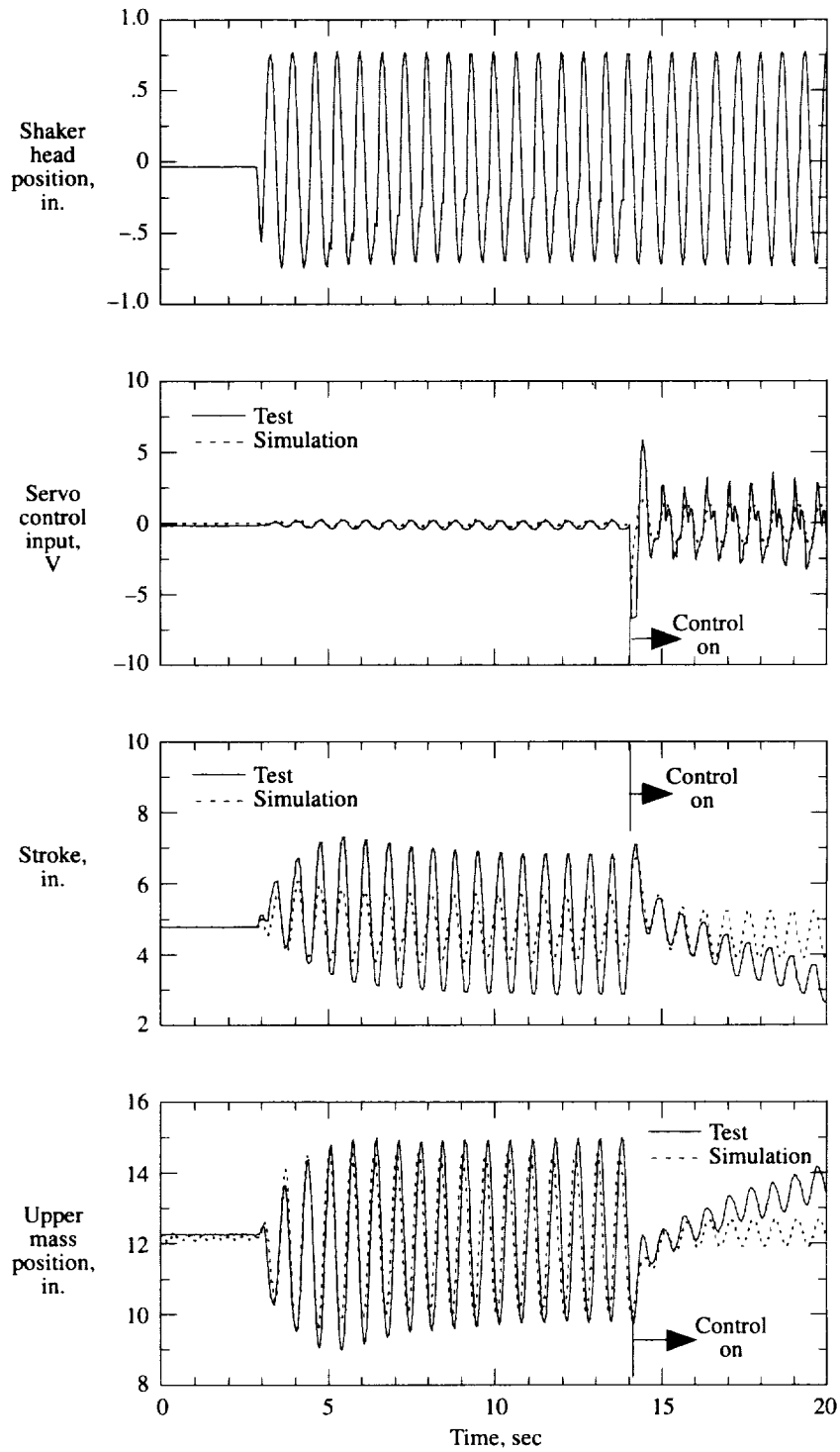Figure 8. Controlled test and analysis results due to periodic disturbance at 1.5 Hz.

Figure 9. Comparison of results to periodic runway disturbance at 1.5 Hz.

14

Axle load feedback is used as a measure of the upper mass motion. This control loop is toggled on and off during an experiment. Data shown in figures 8 and 9 had the axle load feedback loop turned on after 14 s. The upper mass position is reduced to 25 percent of the uncontrolled position after the axle load feedback loop is turned on. Drift after the initiation of control in the stroke and upper mass position histories in figure 9 could be attributed, in part, to a continuous decrease in the control system hydraulic supply pressure. All simulation results assume a constant control system hydraulic supply pressure. To experimentally minimize the effect of reduced control system hydraulic supply pressure, long duration tests were interrupted periodically to allow for the recovery of system hydraulic pressure. Discrepancies in stroke levels between test and simulation are not well understood.

Friction played a key role in unrestrained tests performed with this test bed. To illustrate the problem, figure 10 shows a frequency response function of the upper accelerometer-to-servo command. Note that the landing gear locks above 0.7 Hz due to friction. Control authority is lost beyond 0.7 Hz due to high friction levels, about 2000 lbf statically and 400 lbf dynamically. This static friction level causes a condition in which pressure versus stroke equilibrium can be in error by as much as ±45 psi. Also important is the use of nitrogen in the upper chamber. Nitrogen serves as a soft cushion for load transfer through the gear. In the absence of nitrogen, the strut is full of hydraulic fluid, which is incompressible, and therefore small amounts of hydraulic fluid into or out of the strut cause large changes in the internal pressures. Because the servo hydraulic system has a limited supply of external hydraulic fluid, the absence of nitrogen allows for longer test time and higher forces in the system but requires higher pressures for the external supply.

Controlled tests like the one shown in figures 8 and 9 can be performed only at discrete frequencies with the capabilities of the existing hydraulic system. To test the frequency range between 0.1 Hz to 4 Hz, the spectrum analyzer was set for a sine sweep, and the test was conducted over a long period of time, with periodic stops to allow for the hydraulic system to be resupplied. Open and closed-loop results from this test are shown in figure 11. Note that in this test the shaker table was used as the input disturbance and provided enough energy to prevent the system from locking up below 1.2 Hz. Feedback from position and axle load signals were used in the control system to attenuate responses between 1.5 and 3.5 Hz. The maximum amplitude reduction is a factor of 4.4 at 1.4 Hz, with reductions beyond 3.5 Hz of about 20 percent. Using the strain gauge sensor to measure axle load provides a cleaner signal for feedback and reduces the risk of high-frequency instabilities in the feedback loop. Note that in the ideal case with the control system fully charged, with a gain optimized for a single frequency, and by controlling the system at its natural frequency, amplitude reductions of a factor of 10 have been observed.
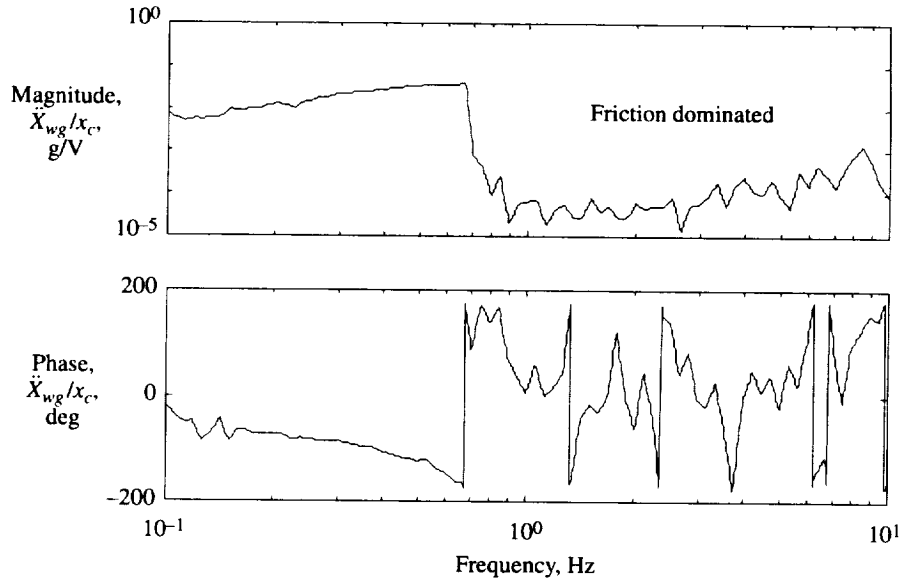
Figure 10. Frequency response from upper servo command to upper accelerometer.
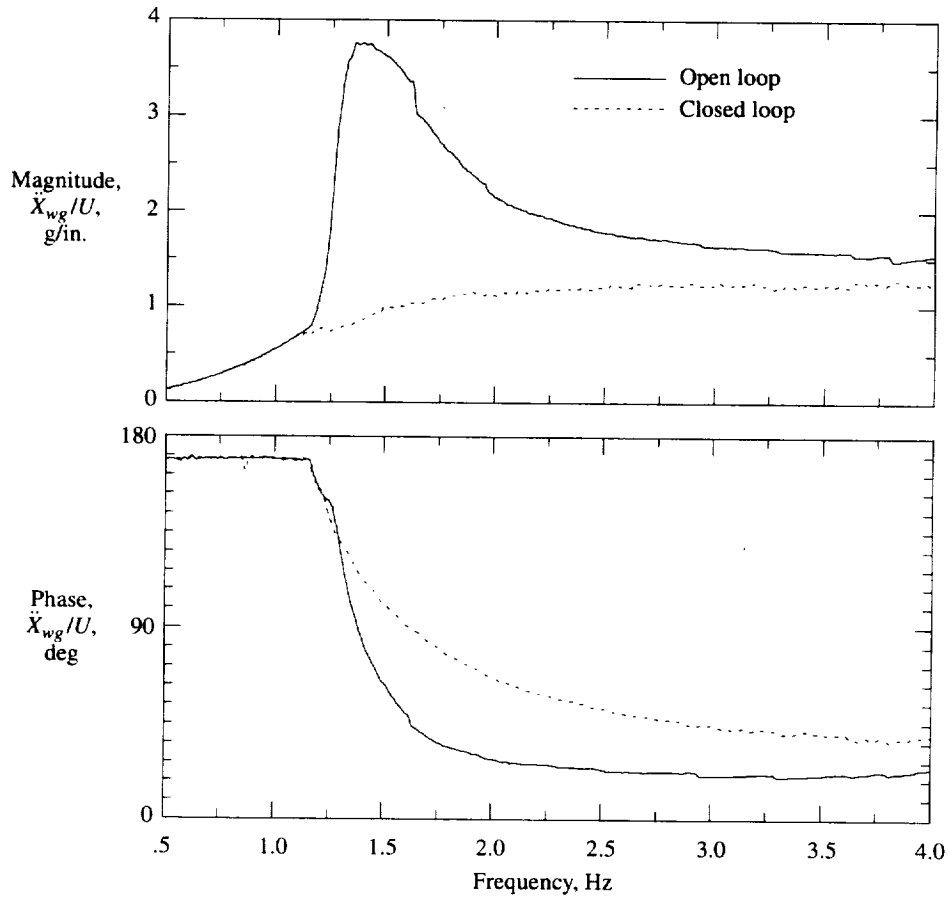

Figure 11. Upper acceleration to shaker position transfer function.

7. Summary

Equations of motion for a telescoping landing gear system have been developed, incorporating an external servohydraulic system that allows for landing gear actuation. The electronic servohydraulic system model combined the electronics and hydraulic dynamics in one relatively simple formulation. This formulation uses an exact internal pressure expression requiring the solution of a multivalue algebraic equation at each time step. At equilibrium, pressures within the strut are balanced at a given stroke position and command flow into or out of the chamber.

A number of aspects of actively controlled landing gear design have been demonstrated in this study. Fuselage vibration reduction levels, by a factor of 4, have been demonstrated, along with some of the fundamental limitations of implementing such systems in landing gear design. High friction levels hindered our ability to achieve higher performance without a major redesign of the gear. However, even modest vibration reductions may translate into reductions in landing gear loads and therefore aircraft structural weight.

Appendix A

Development of Equations of Motion

Fundamental relationships between forces acting on the landing gear and the fluid pressures inside the landing gear are developed in the following sections.

Pneumatic Pressure Equation

The pressure terms that contributed to the forces F_1 and F_2 in equation (3) need to be related to position X_{wg} and X_s or their derivatives. Nitrogen pressure changes have been described (ref. 13) by the polytropic gas law for a closed system as

$$P_u = P_{ni}\left(\frac{V_{ni}^o}{V_{ni}}\right)^{\gamma} \tag{A1}$$

where V_{ni}^o is the initial nitrogen volume, V_{ni} is the actual nitrogen volume, P_{ni} is the initial nitrogen charge pressure, and γ is the polytropic gas constant. This representation of the pressure change is assumed to happen as a quasi-equilibrium process. In most situations the polytropic gas constant is actually not constant and is usually calculated from pressure-stroke data. However, reference 13 showed the experimental estimation of a single value for the polytropic constant. Equation (A1) is defined in such a manner that P_u will become very large for small values of V_{ni}; that is, the gear is nearly collapsed. This equation is a suitable representation of the process, with only the polytropic gas constant γ as an unknown.

Before developing expressions for hydraulic fluid motion between chambers, a fundamental assumption is that the upper chamber hydraulic fluid pressure equals the nitrogen pressure. An expression for the nitrogen volume V_{ni} is now sought. The total volume available in the system is defined by using the dimensions shown in figure A1 as

$$V_T = A_L(L_u - X_s) + A_r X_s \tag{A2}$$

assuming $A_L = A_u$. This volume houses both hydraulic fluid and nitrogen in the system. Since the nitrogen level is given by X_{ni}, with volume computed as $V_{ni} = A_u X_{ni}$, the corresponding volume of hydraulic fluid is given by

$$V_{liq} = V_T - V_{ni} = A_L L_u - (A_L - A_r)X_s - A_L X_{ni} \tag{A3}$$

and the rate of change of the volume of hydraulic fluid is

$$\frac{dV_{liq}}{dt} = -(A_L - A_r)\dot{X}_s - A_L \dot{X}_{ni} \tag{A4}$$

In a closed system, the amount of hydraulic fluid V_{liq} is constant; therefore, the rate of change is zero. Using this fact with equation (A4) yields an expression for the nitrogen level as

$$\dot{X}_{ni} = -\frac{(A_L - A_r)}{A_L}\dot{X}_s \tag{A5}$$
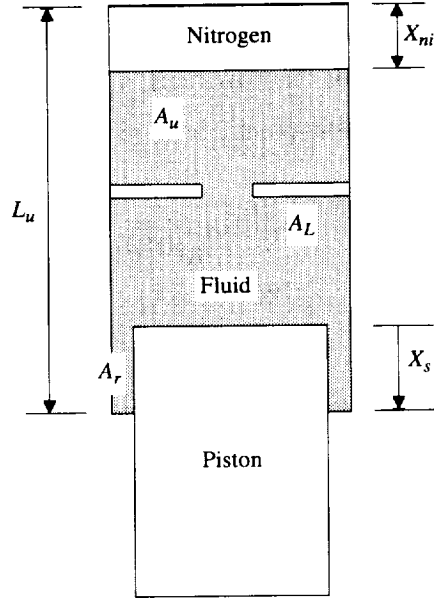
Figure A1. Hydraulic fluid-nitrogen volumetric diagram.

If the system is not closed; for example, if hydraulic fluid is entering or leaving the chamber at a rate Q_c, the rate of change of the volume of hydraulic fluid is given as

$$\frac{dV_{liq}}{dt} = Q_c = -(A_L - A_R)\dot{X}_s - A_L\dot{X}_{ni} \tag{A6}$$

Solving this equation for the nitrogen level yields

$$\dot{X}_{ni} = -\frac{(A_L - A_R)}{A_L}\dot{X}_s - \frac{Q_c}{A_L} \tag{A7}$$

This differential equation, along with the initial value for the nitrogen level X_{ni}^o, describes changes in nitrogen level as a function of time. Canceling the area terms in equation (A1), the upper chamber pressure is now written as

$$P_u = P_{ni}\left(\frac{X_{ni}^o}{X_{ni}}\right)^\gamma \tag{A8}$$

Note that equations (A7) and (A8) relate the stroke to volumetric changes in hydraulic fluid. We will now develop the pressure equations for the system.

Lower Chamber Hydraulic Pressure Equation

Hydraulic fluid pressure in the lower chamber and the snubber chamber is related to the flow rates of the hydraulic fluid into and out of those regions. The volumetric flow rates through the orifice plate hole Q_o and the snubber orifices Q_s can be determined by combining the continuity equation and Bernoulli's equation for fluids. Flow is always from high pressure to low pressure. Bernoulli's equation for an incompressible fluid states that along a streamline $\frac{P}{\vartheta} + \frac{1}{2g}v^2 + z = c$, where P is the pressure at some point, g is the gravitational acceleration, v is the velocity of the flow, ϑ is the specific weight of the fluid, z is the height difference from some zero reference, and c is a constant. This equation assumes

19

that the viscous effects within the fluid are negligible, the flow is steady and incompressible, and only points along a streamline were considered. Examine points 1 and 2 along a streamline; the mass continuity for incompressible fluid states that the flow rates $A_1 v_1 = A_2 v_2$. Assuming that the pressure at point 2 is $P_2 > P_1$ and that the flow is from point 2 to 1, one can solve for the velocity v_1 from the continuity equation as

$$v_1 = \frac{D_2^2}{D_1^2} v_2$$

where the area in the continuity equation is now expressed in terms of diameters. Substituting this velocity into the Bernoulli equation yields

$$v_1 = \pm \sqrt{\frac{2(P_2 - P_1)}{\rho \left(1 - \frac{D_1^4}{D_2^4} \right)}} \tag{A9}$$

The ideal volumetric flow rate (Q_{ideal}) for an incompressible fluid can be expressed as $Q_{ideal} = Av$. In a realistic flow situation though, there is a flow rate loss due to flow restrictions in the orifice. This loss is empirically quantified by a discharge coefficient C_d, which represents the percentage of the ideal flow that actually occurs. This coefficient, when multiplied by the ideal flow, yields

$$Q_{real} = C_d Q_{ideal} = A C_d v \tag{A10}$$

Substituting the velocity in equation (A9) into equation (A10)

$$Q_{real} = A C_d \sqrt{\frac{2}{\rho \left[1 - \left(\frac{D_1}{D_2} \right)^4 \right]}} \sqrt{P_2 - P_1}; \; for \; P_2 > P_1 \tag{A11}$$

For the landing gear shown in figure 1, there are three flows that are of concern: the flow through the orifice plate Q_o, flow in and out of the snubber chamber Q_s, and if the gear is actuated externally, there is an additional flow Q_c. The Q_c is supplied by an external high- and low-pressure reservoir, which adds or removes hydraulic fluid from the system.

Defining a control volume as shown by the dashed line in figure A2, compression occurs when $\dot{X}_s > 0$, and extension occurs when $\dot{X}_s < 0$. Flow is assumed to be positive leaving the control volume and negative entering it. For an incompressible fluid, continuity yields

$$Q_c + Q_o + Q_s = A_L \dot{X}_s \tag{A12}$$

Equation (A12) defines the general form of the continuity equation. Because flow directions have to be taken into account explicitly to determine pressures in the various chambers, one needs to consider all
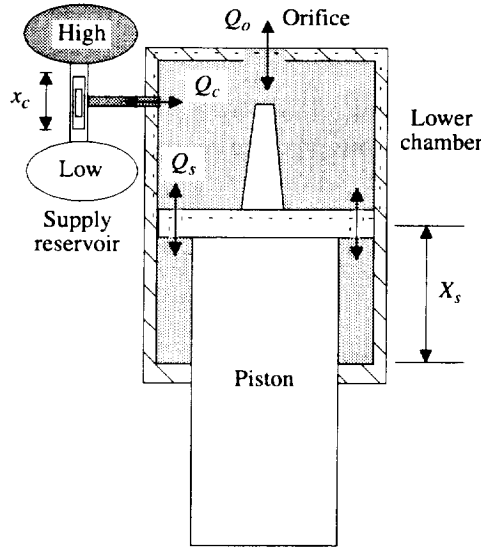
20

Figure A2. Control volume between piston and orifice plate.

possibilities. Flow in or out of the snubber chamber always equals the volume displaced during expansion or compression $Q_s = A_R \dot{X}_s$. Substituting this value into equation (A12) yields

$$Q_c + Q_o = (A_L - A_R)\dot{X}_s \tag{A13}$$

Substituting the appropriate pressures, areas, and diameters into equation (A11), the flow rate through the orifice plate during the compression $\dot{X}_s > 0$ can be written as

$$Q_o = A_o C_d \sqrt{\frac{2}{\rho\left[1 - \left(\dfrac{D_o}{D_L}\right)^4\right]}} \sqrt{P_L - P_u}, \quad P_L > P_u \tag{A14}$$

where D_o is the effective diameter of the main orifice, D_L is the diameter of the lower chamber, C_d is the discharge coefficient of the main orifice, and A_o is the effective area of the main orifice. To simplify equation (A14), the nonpressure terms were grouped as

$$E_1 = A_o C_d \sqrt{\frac{2}{\rho\left[1 - \left(\dfrac{D_o}{D_L}\right)^4\right]}}$$

The flow through the orifice is now written as

$$Q_o = E_1 \sqrt{P_L - P_u} \quad \text{for} \quad P_L > P_u \tag{A15}$$

21

Obviously, if the upper chamber pressure is higher than the lower chamber pressure, the order of the pressure terms must be reversed.

To actuate the piston, one can add or remove hydraulic fluid from the landing gear. Considering a system with infinitely large high- and low-pressure reservoirs, depicted in figure A2, an external flow into the lower chamber can be written as

$$Q_c^i = -C_c x_c \sqrt{P_{High} - P_L} \qquad x_c < 0 \tag{A16}$$

and flow out of the lower chamber is given by

$$Q_c^o = C_c x_c \sqrt{P_L - P_{Low}} \qquad x_c > 0 \tag{A17}$$

where x_c is a command variable, and the parameter C_c combines empirically determined values for the discharge coefficient, orifice area, and flow gain per unit command input. Superscripts i or o are used to distinguish inflow from outflow. To evaluate the pressures, one needs to examine the different flow directions in the control volume.

Figure A3 shows three potential flow directions for Q_c and Q_o for the compression case. The corresponding continuity equations for $\dot{X}_s > 0$ are

$$Q_o - Q_c^i = E_1 \sqrt{P_L - P_u} + C_c x_c \sqrt{P_{High} - P_L} = (A_L - A_R)\dot{X}_s; \quad x_c < 0, Q_o > 0$$

$$Q_o + Q_c^o = E_1 \sqrt{P_L - P_u} + C_c x_c \sqrt{P_L - P_{Low}} = (A_L - A_R)\dot{X}_s; \quad x_c > 0, Q_o > 0 \tag{A18}$$

$$-Q_o + Q_c^o = -E_1 \sqrt{P_u - P_L} + C_c x_c \sqrt{P_L - P_{Low}} = (A_L - A_R)\dot{X}_s; \quad x_c > 0, Q_o < 0$$

Similarly, the extension case has three potential flow directions shown in figure A4 with corresponding flow equations for $\dot{X}_s < 0$:

$$-Q_o - Q_c^i = E_1 \sqrt{P_u - P_L} + C_c x_c \sqrt{P_{High} - P_L} = (A_L - A_R)\dot{X}_s; \quad x_c < 0, Q_o < 0$$

$$-Q_o + Q_c^o = -E_1 \sqrt{P_u - P_L} + C_c x_c \sqrt{P_L - P_{Low}} = (A_L - A_R)\dot{X}_s; \quad x_c > 0, Q_o < 0 \tag{A19}$$

$$Q_o + Q_c^i = E_1 \sqrt{P_L - P_u} + C_c x_c \sqrt{P_{High} - P_L} = (A_L - A_R)\dot{X}_s; \quad x_c < 0, Q_o > 0$$
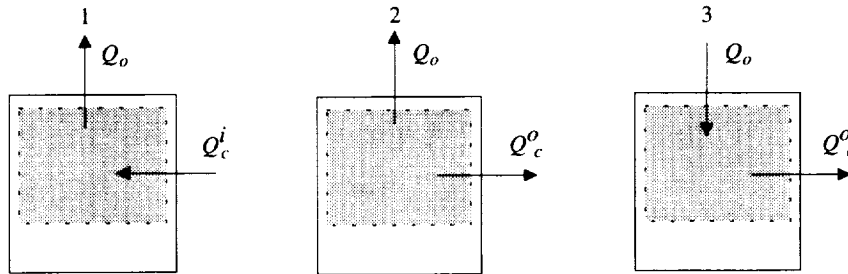
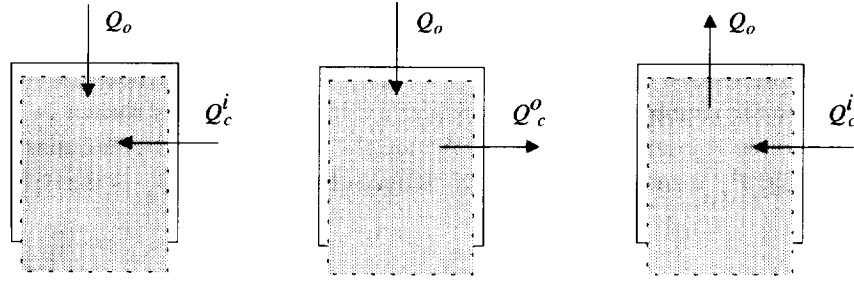Figure A3. Potential flow directions for compression case $\dot{X}_s > 0$.

Figure A4. Potential flow directions for extension case $\dot{X}_s < 0$.

Equations (A8), (A18), and (A19) need to be solved simultaneously to determine the pressures P_L and P_u. Note that equations (A7) and (A8) couple the upper pressure to the flow rate Q_c. Appendix B shows an explicit solution for the lower pressure P_L, obtained by using the Mathematica Symbolic manipulation program (The Mathematica Book, third ed., Wolfram Media, Cambridge University Press), reference 15.

A case not considered thus far is when the system is locked due to friction; that is, $\dot{X}_s = 0$ (lower and upper chambers move together). When no external hydraulic fluid source is in use, $x_c = 0$; there is no hydraulic fluid transfer between chambers. However, when an external source is in use, hydraulic fluid transfer is determined by continuity $Q_o = Q_c$. Two hydraulic fluid flow cases are possible depending upon the control variable x_c value; they are

$$-Q_o = -E_1\sqrt{P_L - P_u} = Q_c^i = -C_c x_c \sqrt{P_{High} - P_L} \; , \; x_c < 0, \, Q_o < 0$$

$$Q_o = E_1\sqrt{P_u - P_L} = Q_c^o = C_c x_c \sqrt{P_L - P_{Low}} \; , \; x_c > 0, \, Q_o > 0$$

(A20)

Solving equation (A20) for the lower chamber pressure yields

$$P_L = \frac{\left(\dfrac{E_1}{C_c x_c}\right)^2 P_u + P_{High}}{\left(\dfrac{E_1}{C_c x_c}\right)^2 + 1} \quad \text{for} \quad x_c < 0$$

$$P_L = \frac{\left(\dfrac{E_1}{C_c x_c}\right)^2 P_u + P_{Low}}{\left(\dfrac{E_1}{C_c x_c}\right)^2 + 1} \quad \text{for} \quad x_c > 0$$

(A21)

Most of the pressures needed to solve equation (3) have been developed, except for the snubber chamber pressure. In the following section, these expressions are developed.

Snubber Chamber Hydraulic Pressure Equation

The analysis in this section is similar to the lower chamber analysis just described. To develop pressure relationships for the snubber chamber, consider a control volume as shown by the dashed line in figure A5. The variables A_R and D_R in figure A5 are the snubber chamber annular area and effective diameter, respectively; P_s is the pressure in the snubber chamber, and D_s is the diameter of the snubber orifices.

In general, the continuity equation relates the flow in or out of the snubber to the volumetric change as follows:

$$Q_s = A_R \dot{X}_s \tag{A22}$$

Flow into the control volume of the snubber area during a compression mode $\dot{X}_s > 0$ is given by

$$Q_s = A_s C_{dS} \sqrt{\frac{2}{\rho \left[1 - \left(\dfrac{D_s}{D_L} \right)^4 \right]}} \sqrt{P_L - P_s}, \quad P_L > P_s$$

$$= E_2 \sqrt{P_L - P_s} \tag{A23}$$

where C_{dS} is the discharge coefficient of the snubber orifices, and A_s is the effective area of the snubber orifice. For the extension mode $\dot{X}_s < 0$, the flow is into the control volume and equation (A23) yields

$$Q_s = -A_s C_{dS} \sqrt{\frac{2}{\rho \left[1 - \left(\dfrac{D_s}{D_R} \right)^4 \right]}} \sqrt{P_s - P_L}, \quad P_s > P_L$$
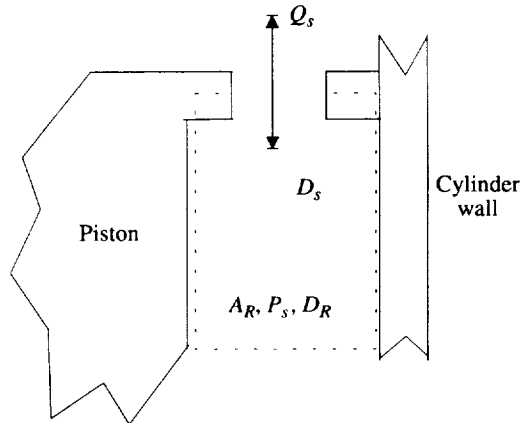
$$= -E_3 \sqrt{P_s - P_L} \tag{A24}$$

Figure A5. Control volume for snubber chamber.

24

where D_R is the effective diameter of the annular snubber chamber. Often the snubber orifice diameter D_s is different in extension and compression. For those cases, the appropriate diameters need to be used in this equation for each case. Equations (A23) and (A24) can be used to determine the snubber pressure, given a flow rate Q_s. Substituting the flow rate Q_s in equations (A23) and (A24) into equation (A22) yields

$$E_2 \sqrt{P_L - P_s} = A_R \dot{X}_s \quad \text{for} \quad \dot{X}_s > 0$$
$$-E_3 \sqrt{P_s - P_L} = A_R \dot{X}_s \quad \text{for} \quad \dot{X}_s < 0$$

(A25)

Solving for the snubber pressures

$$P_s = P_L - \left(\frac{A_R}{E_2}\right)^2 \dot{X}_s^2 \quad \text{for} \quad \dot{X}_s > 0$$

$$P_s = P_L + \left(\frac{A_R}{E_3}\right)^2 \dot{X}_s^2 \quad \text{for} \quad \dot{X}_s < 0$$

(A26)

Equations (A8), (A18), (A19), and (A26) provide the fundamental relationships between the pressures, displacements, and commanded input x_c. To evaluate the time responses for all these quantities, equations (3) and (A7) must be integrated in time with appropriate initial conditions for all variables. Friction models will now be described.

Friction Models

The only unknown term left in equation (3) is friction. Friction in this landing gear comes mainly from two sources: friction due to tightness of the seal and friction due to the offset wheel (moment). The seal friction has a maximum value when the system is locked and decreases as the system begins to move. The functional relationship between frictional force level and velocity is determined through testing. The friction due to the offset wheel is the result of the moment produced by the nonaxially loaded piston within the cylinder.

Figure A6 shows that the force between the piston head and the cylinder N is a result of the tire force F_t applied at a distance l from the centerline of the piston. The frictional force due to the offset wheel is

$$F_{ow} = \mu N$$

(A27)

where N is the normal force on the cylinder wall resisting motion of the piston head, and μ is the coefficient of friction between the two parts. The normal force N is computed by adding the moments about point O; β is defined as one-half the thickness of the lower bearing. Solving for the normal force N and substituting into equation (A27) yields

$$F_{ow} = \mu \left(\frac{l F_t}{X_s + \beta}\right)$$
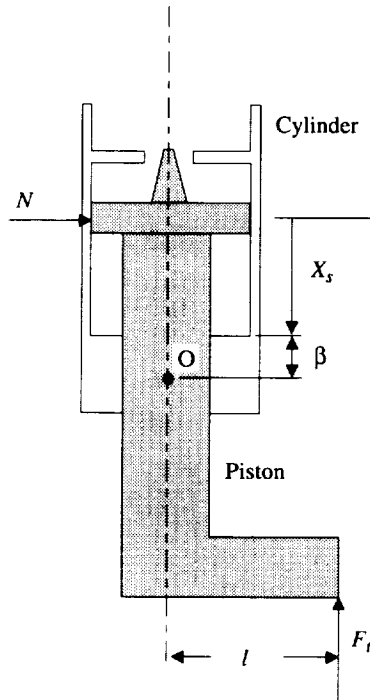
(A28)

25

Figure A6. Schematic of landing gear friction model development.

The total friction force in the landing gear f is given by

$$f = F_{seal} + F_{ow} \tag{A29}$$

Friction effects were included in the numerical simulations by using the approach described in reference 16.

Note that this model takes into account only vertical loads on the strut. Furthermore, the tire is modeled as a nonlinear spring and damper combination and does not take into account radial stiffening due to centripetal forces. Also, all structural members were assumed to be rigid, each having only a vertical degree of freedom. These assumptions are adequate for taxiing over runway profiles and for landing impact (spin-up drag on the tire does not significantly affect the vertical loads on the strut). Any braking or turning maneuvers were not covered in the development. The equations developed here are the basis for a "rollout" simulation.

Appendix B

Analytical Solution of Pressure Equation

All possible sign combinations in equations (A18) and (A19) can be considered by using a generic form such as

$$c_1\sqrt{P_L - P_u} + c_2\sqrt{P_L - P_r} = c_3 \tag{B1}$$

$$c_1\sqrt{P_u - P_L} + c_2\sqrt{P_L - P_r} = c_3 \tag{B2}$$

$$c_1\sqrt{P_u - P_L} + c_2\sqrt{P_r - P_L} = c_3 \tag{B3}$$

Solutions for these three equations have the following form:

$$P_L = \frac{c_2^2 c_3^2 + c_2^4 P_r \pm 2c_1 c_2 c_3 \sqrt{c_3^2 - \left(c_1^2 - c_2^2\right)(P_r - P_u) + c_1^4 P_u + c_1^2\left[c_3^2 - c_2^2(P_r + P_u)\right]}}{\left(c_1^2 - c_2^2\right)^2} \tag{B4}$$

$$P_L = \frac{c_2^2 c_3^2 + c_2^4 P_r \pm 2c_1 c_2 c_3 \sqrt{\left(c_1^2 + c_2^2\right)(P_u - P_r) - c_3^2 + c_1^4 P_u + c_1^2\left[-c_3^2 + c_2^2(P_r + P_u)\right]}}{\left(c_1^2 + c_2^2\right)^2} \tag{B5}$$

$$P_L = \frac{-c_2^2 c_3^2 + c_2^4 P_r \pm 2c_1 c_2 c_3 \sqrt{c_3^2 + \left(c_1^2 - c_2^2\right)(P_r - P_u) + c_1^4 P_u - c_1^2\left[c_3^2 - c_2^2(P_r + P_u)\right]}}{\left(c_1^2 - c_2^2\right)^2} \tag{B6}$$

These are potential solutions for equations (B1), (B2), and (B3), respectively. It is important to realize that physically realistic solutions may not exist for certain values of the parameters, c_1, c_2, c_3, and the pressures.

References

1. Currey, Norman S.: *Aircraft Landing Gear Design: Principles and Practices.* AIAA Educ. Ser., AIAA, 1998.

2. Milwitzky, Benjamin; and Cook, Francis E.: *Analysis of Landing-Gear Behavior.* NACA Rept. No. 1154, 1953.

3. Ottens, H. H.: Predicted and Measured Landing Gear Loads for the NF-5 Aircraft Taxiing Over Bumpy Runway. *Aircraft Dynamic Response to Damage and Repaired Runways,* AGARD CP-326, 1982.

4. Payne, B. W.; Dudman, A. E.; Morris, B. R.; and Hockenhull, M.: Development of a Cost Effective Approach to Modeling Aircraft Response to Repaired Runways. *Aircraft Dynamic Response to Damaged and Repaired Runways,* AGARD-CP-326, 1982.

5. Freymann, R.: *An Experimental-Analytical Routine for the Dynamic Qualification of Aircraft Operating on Rough Runway Surfaces.* AGARD R-731, 1987.

6. Gerardi, Tony G.; and Minnetyan, Levon: Status of Computer Simulations of USAF Aircraft and an Alternative Simulation Technique. *Aircraft Dynamic Response to Damaged and Repaired Runways,* AGARD-CP-326, 1982, pp. 11-1–11-10.

7. Freymann, Raymond; and Johnson, William P.: Simulation of Aircraft Taxi Testing on the Agile Shaker Test Facility. *Second International Symposium on Aeroelasticity and Structural Dynamics,* DGLR/DFVLR/NLR/ONERA, 1985, pp. 468–476.

8. Shepherd, Alan; Catt, Tyrone; and Cowling, David: *An Aircraft Landing Gear Simulation Parametric Leg Model.* SDL Rept. No. 234, Stirling Dynamics Limited, 1993.

9. Catt, Tyrone; Cowling, David; and Shepherd, Alan: *Active Landing Gear Control for Improved Ride Quality During Ground Roll.* SDL Rept. No. 232, Stirling Dynamics Limited, 1992.

10. Ross, Irving; and Edson, Ralph: *An Electronic Control for an Electrohydraulic Active Control Aircraft Landing Gear.* NASA CR-3113, 1979.

11. Ross, Irving; and Edson, Ralph: *An Electronic Control for an Electrohydraulic Active Control Landing Gear for the F-4 Aircraft.* NASA CR-3552, 1982.

12. Freymann, Raymond: *Actively Damped Landing Gear System.* Landing Gear Design Loads, AGARD CP-484, 1990.

13. Daniels, James N.: *A Method for Landing Gear Modeling and Simulation With Experimental Validation.* NASA CR-201601, 1996.

14. *SIMULINK—Dynamic System Simulation for MATLAB®.* Version 2—Using SIMULINK, The Math Works Inc., 1997.

15. Wolfram, Stephen: *The Mathematica Book®.* Wolfram Media/Cambridge Univ. Press, 1996.

16. Karnopp, Dean: Computer Simulation of Stick-Slip Friction in Mechanical Dynamic Systems. *J. Dyn. Syst., Meas., & Control,* vol. 107/103, 1985.

REPORT DOCUMENTATION PAGE

1. AGENCY USE ONLY (Leave blank)	2. REPORT DATE	3. REPORT TYPE AND DATES COVERED
	May 1999	Technical Publication

4. TITLE AND SUBTITLE
Modeling and Validation of a Navy A6-Intruder Actively Controlled Landing Gear System

5. FUNDING NUMBERS
WU 522-18-11-04

6. AUTHOR(S)
Lucas G. Horta, Robert H. Daugherty, and Veloria J. Martinson

7. PERFORMING ORGANIZATION NAME(S) AND ADDRESS(ES)
NASA Langley Research Center
Hampton, VA 23681-2199

8. PERFORMING ORGANIZATION REPORT NUMBER
L-17817

9. SPONSORING/MONITORING AGENCY NAME(S) AND ADDRESS(ES)
National Aeronautics and Space Administration
Washington, DC 20546-0001

10. SPONSORING/MONITORING AGENCY REPORT NUMBER
NASA/TP-1999-209124

11. SUPPLEMENTARY NOTES

12a. DISTRIBUTION/AVAILABILITY STATEMENT
Unclassified–Unlimited
Subject Category 05   Distribution: Standard
Availability: NASA CASI (301) 621-0390

12b. DISTRIBUTION CODE

13. ABSTRACT (Maximum 200 words)

Concepts for long-range air travel are characterized by airframe designs with long, slender, relatively flexible fuselages. One aspect often overlooked is ground-induced vibration of these aircraft. This paper presents an analytical and experimental study of reducing ground-induced aircraft vibration loads by using actively controlled landing gear. A facility has been developed to test various active landing gear control concepts and their performance. The facility uses a Navy A6 Intruder landing gear fitted with an auxiliary hydraulic supply electronically controlled by servo valves. An analytical model of the gear is presented, including modifications to actuate the gear externally, and test data are used to validate the model. The control design is described and closed-loop test and analysis comparisons are presented.

14. SUBJECT TERMS
Vibration; Active control; Landing gear; Aircraft

15. NUMBER OF PAGES
33

16. PRICE CODE
A03

17. SECURITY CLASSIFICATION OF REPORT	18. SECURITY CLASSIFICATION OF THIS PAGE	19. SECURITY CLASSIFICATION OF ABSTRACT	20. LIMITATION OF ABSTRACT
Unclassified	Unclassified	Unclassified	UL